Heat Mass Transfer (2018) 54:2433–2442
DOI 10.1007/s00231-017-2101-9

ORIGINAL

Investigation of heat transfer inside a PCM-air heat exchanger: a numerical parametric study

Florent Herbinger[1] · **Maha Bhouri**[1] · **Dominic Groulx**[1]

Received: 21 March 2017 / Accepted: 6 July 2017 / Published online: 21 July 2017

Abstract In this paper, the use of PCMs for thermal storage of energy in HVAC applications was investigated by studying numerically the thermal performance of a PCM-air heat exchanger. The PCM used in this study was dodecanoic acid. A symmetric 3D model, incorporating conductive and convective heat transfer (air only) as well as laminar flow, was created in COMSOL Multiphysics 5.0. Simulations examined the dependence of the heat transfer rate on the temperature and velocity of the incoming air as well as the size of the channels in the heat exchanger. Results indicated that small channels size lead to a higher heat transfer rates. A similar trend was also obtained for high incoming air temperature, whereas the heat transfer rate was less sensitive to the incoming air velocity.

Abbreviations

HVAC	Heating, Ventilation, and Air Conditioning
PCM	Phase Change Material
TES	Thermal Energy Storage

Nomenclature

A	Area (m^2)
$B(T)$	Melt Fraction
C_p	Specific Heat Capacity (J kg^{-1} K^{-1})
$D(T)$	Gaussian Distribution of the Latent Heat of Fusion
k	Thermal Conductivity (W m^{-1} K^{-1})
L	Latent Heat of Fusion (J kg^{-1})
N	Number of Square Channels
p	Pressure (Pa)
P	Wetted Perimeter (m)
q”	Heat Flux (W m^{-2})
Q	Heat Transfer Rate (W)
Re	Reynolds Number
t	Time (s)
T	Temperature (K)
u	Velocity (m s^{-1})

Greek letters

ρ	Density (kg m^{-3})
μ	Viscosity (Pa s)
ΔT	Temperature Difference (K)

Subscripts

ch	Channel
in	Inlet
l	Liquid
m	Melting
out	Outlet
s	Solid

1 Introduction

Heating, ventilation, and air-conditioning (HVAC) systems help provide thermal comfort and good air quality in residential and commercial buildings. However, this often comes at the expense of emitting large amounts of greenhouse gases due to the consumption of fossil fuels [1]. In this context, serious efforts have been devoted to improving the operation and efficiency of HVAC systems. Among the developed technologies [2, 3], phase change materials (PCMs)-based Thermal Energy Storage (TES) Systems have proven to have great potential for reducing HVAC energy consumption and

✉ Dominic Groulx
dominic.groulx@dal.ca

[1] Mechanical Engineering Department, Dalhousie University, Halifax, NS, Canada

its environmental impact, due to their high energy storage densities and nearly constant operating temperatures. In particular, the use of PCM-air TES systems in combination with HVAC forced air systems are of great relevance to the cooling and heating of buildings. One of their operating principles consists of cooling down warm air entering a building during the day by exchanging heat with the PCM. This heat is then recovered by low temperature air at night time.

Numerous studies of PCM-air based TES free cooling systems indicate that the limited heat transfer between the air and the PCM-TES unit is the major bottleneck to successfully integrating these systems in low-energy buildings [3, 4]. This is mainly due to the low thermal conductivity of the PCM, making its melting and solidification processes excessively slow; hence, the overall heat transfer rates during charging and discharging are often too low for this type of application.

In order to address this "rate problem", the heat exchanged between the air and PCM inside the TES unit has to be optimized, which amongst other things, is related to the selection of the PCM-air heat exchanger geometry. Indeed, a variety of configurations for PCM to air heat exchange have been investigated: PCM slabs with rectangular air flow channels in-between [5–16]; annular PCM tube with internal air flow [17] or tube banks with air driven across them [18]; cylindrical PCM shells with air flowing through tubes [19, 20]; and packed spherical PCM capsules with air passing through in a cylindrical reactor [21].

Among these various PCM-air heat exchanger configurations, the one with PCM slabs and air gaps is the most studied for thermal energy storage in building ventilation systems. Previous research has covered both experimental studies of small-scale and real-scale prototypes, including tests done in buildings [7, 8, 10, 16, 22], and numerical analysis [8, 10, 11, 14, 22], which has served as a tool for further optimization of the heat storage system. The main focus was on identifying a compromise between the amount of heat to be stored and the time required for the melting/solidification process. To this end, various parameters were explored [5–10], including amounts and types of PCM, operating conditions, such as the temperature and flow rate of the incoming air, and geometric properties of the PCM-air storage unit, such as the thickness of the PCM slabs and the fluid passage gap.

Vakilaltojjar and Saman [5] studied a phase-change energy storage system consisting of sections of two inorganic PCMs. The PCMs were placed in thin flat containers separated by gaps where air was flowing. Results showed that the air velocity profile has a small influence on the heat transfer characteristics and the outlet air temperature. A better performance of the studied system was achieved by using smaller air gaps and thinner PCMs slabs; however, this also resulted in the increase of the number of PCMs slabs and the total volume of the storage system, and a higher pressure drop across the air passage was reported.

Lazaro et al. [6] developed a real-scale prototype of a PCM-air heat exchanger. From the experimental results, an empirical model was used to determine the required melting temperature of the PCM for a specific heating power in order to maintain a constant temperature for the targeted application.

Zalba et al. [7] developed and tested a PCM-air heat exchanger consisting of flat plates of PCMs separated by air channels. A statistical analysis showed that the melting process was more sensitive to the inlet air temperature than the thickness of the encapsulated PCMs. Dolado et al. [8] studied a real scale PCM-air heat exchanger based on a slab macroencapsulated PCM with bulges. A one-dimensional mathematical model taking into account temperature-dependent PCM properties and natural convection, using effective thermal conductivity, was validated and used in a parametric study. It was concluded that increasing the rugosity of the PCM slabs, decreasing the size of air and PCM containers, and increasing the airflow rate can improve the thermal performance of the heat exchanger.

Mosaffa et al. [9] conducted a numerical study to investigate the performance of a TES unit using slabs filled with multiple PCMs. The mathematical model was based on the method of effective heat capacity, and assumed constant thermophysical properties of the PCMs and no natural convection inside its liquid phase. Geometrical parameters of the TES unit were optimized for Iran's climate, resulting in a higher performance than an air conditioning system. Labat et al. [10] developed and tested a PCM-air heat exchanger prototype where a paraffin PCM was distributed into vertical plane-parallel aluminum containers. Fins were introduced between the air blocks to increase the heat exchange between PCM and air. Due to the simple global behavior of the heat exchanger, it was concluded that a simplified numerical model could be used for a further optimization of the performance of the designed TES system.

In this paper, a PCM-air heat exchanger configuration inspired in part by this previous work was modelled. However, a cellular structure where square PCM and air channels were alternated was considered. This configuration was adapted from basic air-to-air heat exchanger design, typically used in heat recovery ventilation systems [23]. The main objective was to assess the thermal performance of such a heat exchanger design as a function of its geometrical properties and its operating conditions; in this case, the thermal performance was centered on the heat transfer rate in order to address the "rate problem" encountered in most PCM-based TES applications [4]. To this end, a three-dimensional numerical model considering heat transfer by conduction in the PCM media and heat transfer by conduction and convection in the air domain with laminar air flow was built and solved using the commercial finite element software, COMSOL Multiphysics 5.0.

The following section of this paper deals with a detailed description of the studied geometry, the mathematical model, and the mesh selection. In the third section, the behavior of the PCM during the melting process and the dependence of the heat transfer rate on the size of the square channels as well as the temperature and velocity of the incoming air are presented and discussed. The paper ends with a general conclusion of the work.

Table 1 Thermophysical properties of dodecanoic acid [24]

Density	885 kg/m^3
Heat Capacity (Solid)	2180 J/kg·K
Heat Capacity (Liquid)	2390 J/kg·K
Latent Heat of Fusion	187,200 J/kg
Thermal Conductivity	0.15 W/m·K
Melting Point	43.5 °C

2 Methodology

2.1 Physical model

As described earlier, the studied geometry replicated a cellular air-to-air heat exchanger. However, every fresh incoming air channel was replaced with PCM, giving a checkerboard pattern. When hot extracted air flowed through the heat exchanger, the heat was transferred to the PCM, leading to melting. When the stored heat would be required, a cold air stream would flow through the PCM-air heat exchanger to absorb the heat from the PCM. The entire geometry of the PCM-air heat exchanger is shown in Fig. 1a). Using symmetry considerations, only one full and four quarter PCM channels (purple) and four half air channels (grey) needed to be simulated, as illustrated in Fig. 1b). Having an expected thermal conductivity much higher than the PCM, the thin heat exchanger walls were not modelled for simplicity in this study.

The PCM used for this study was dodecanoic acid, with a melting temperature of 43.5 °C. Tables 1 and 2 present the thermophysical properties of the PCM and air used in the simulations. For this first parametric study, dry air was considered although it is understood that in HVAC systems, wet air will be moving through the heat exchanger. However, the temperature difference between the air and PCM is what drives the heat transfer rate inside the storage system and this temperature difference will be the same for dry or wet air. Wet air would however result in air cooling slightly slower because of the additional energy found in the water vapor, and therefore cause a slight overall increase in the average temperature difference between the air and PCM, resulting in an increased heat transfer rate. Overall, dry air still accurately captures the important physics phenomena and trends.

The system was studied by varying the dimension of the square PCM and air channel edges, from 2 to 4 to 6 cm, while their length stayed constant at 30 cm (refer to Fig. 1). The PCM domain had an initial temperature of 20 °C, while the inlet temperature of the air was varied between 60 °C and 70 °C. The inlet air velocity was also varied between 0.75 m/s and 1 m/s assuming a laminar flow in the air domain. Considering a square channel with the hydraulic diameter $\frac{4A}{P}$, where A is the cross-sectional area and P is the wetted perimeter, the largest Reynolds number based on the hydraulic diameter was calculated to be 3180 for the largest channel (6 cm edge length) and fastest flow (1 m/s). Based on this number, and for simplicity, this parametric study considered laminar flow even for the highest Re configuration, since the flow regime is just above the early critical Re. Due to the selection of pure laminar flow, no transitional regime could be simulated. The second assumption was to neglect the effect of natural convection in the PCM domain during the melting process. Three dimensional transient simulations including phase change and natural convection require heavy computations

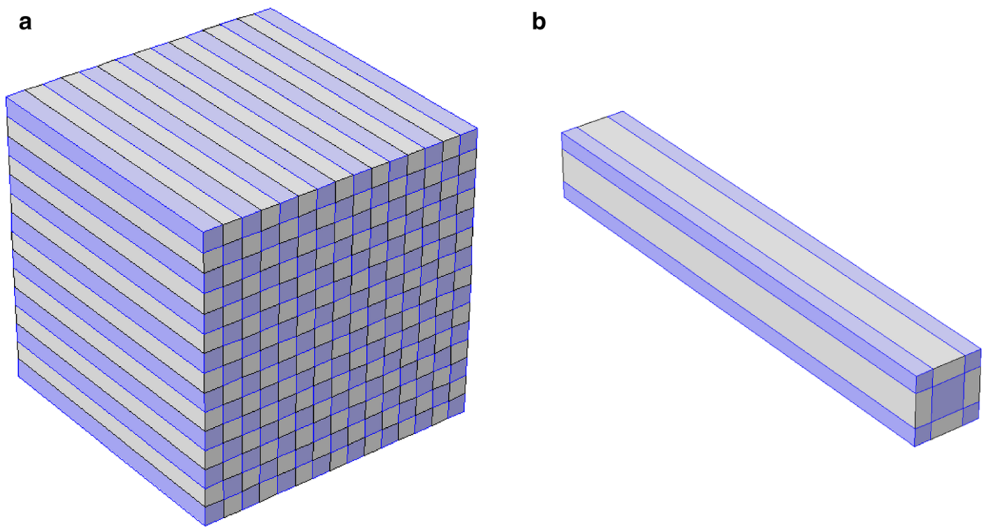

Fig. 1 **a** The entirety of the PCM-air heat exchanger, **b** The geometry with symmetry used as the domain in the study

Table 2 Thermophysical properties of dry air

	60 °C	70 °C
Density	1.060 kg/m^3	1.029 kg/m^3
Heat Capacity	1008 J/kg·K	1009 J/kg·K
Dynamic Viscosity	2.006×10^{-5} Pa·s	2.051×10^{-5} Pa·s
Thermal Conductivity	0.028 W/m·K	0.029 W/m·K

leading to excessively long computational times, which is counter-productive to parametric studies. Additionally, natural convection would play a smaller role in smaller compartments; therefore, it can be neglected without affecting the conclusions drawn from this study.

The values of all parameters varied in this study are summarized in Table 3. Through the changes in the channel's size and inlet air temperature and velocity, the dependence of the heat transfer rate on the geometrical properties and the operating conditions could be determined.

2.2 Mathematical formulation

Within the PCM and air domains, the energy equation applies:

$$\rho C_p \frac{\partial T}{\partial t} + \nabla \cdot (-k\nabla T) + \rho C_p \boldsymbol{u} \cdot \nabla T = 0 \tag{1}$$

where the fluid velocity $\boldsymbol{u}$ is always zero in the PCM domain and is determined from solving the Navier-Stokes equations for the air domain:

$$\frac{\partial \rho}{\partial t} + \nabla \cdot (\rho \boldsymbol{u}) = 0$$
$$\rho \frac{\partial \boldsymbol{u}}{\partial t} + \rho(\boldsymbol{u} \cdot \nabla)\boldsymbol{u} = \nabla \cdot \left[\mu\left(\nabla \boldsymbol{u} + (\nabla \boldsymbol{u})^{\mathrm{T}}\right)\right] - \nabla p \tag{2}$$

The melting process can be modeled by modifying the overall heat capacity of the PCM to account for the large amount of energy provided by the latent heat of fusion, L, once the melting temperature, T_m is attained [25]. The resulting change in the specific capacity of the PCM during its melting is described by defining the two functions, $B(T)$ and $D(T)$ given by:

Table 3 List of varied parameters

Channel edge length (cm)	Area of one inlet channel (m^2), $A_{air.ch}$	Number of air channels, $N_{air.ch}$	Heat transfer area (m^2), $A_{PCM\text{-}air}$	Inlet air temperature (°C)	Inlet air velocity (m/s)
6	0.0036	12	0.72	60, 70	0.75, 1
4	0.0016	28	1.26	60, 70	0.75, 1
2	0.0004	112	2.52	60, 70	0.75, 1

$$B(T) = \begin{cases} 0 & , T < (T_m - \Delta T/2) \\ \dfrac{T - T_m + \Delta T/2}{\Delta T} & , (T_m - \Delta T/2) < T < (T_m + \Delta T/2) \\ 1 & , T > (T_m + \Delta T/2) \end{cases} \tag{3}$$

$$D(T) = \frac{exp\left[-(T - T_m)^2/(\Delta T/4)^2\right]}{\sqrt{\pi(\Delta T/4)^2}} \tag{4}$$

$B(T)$ represents the liquid fraction in the PCM domain. Equation (3) shows that $B(T)$ is equal to 0 in the solid phase, 1 in the liquid phase and varies linearly from 0 to 1 through the transition zone over a temperature interval, ΔT. $D(T)$ is a Gaussian function that accounts for the latent heat of fusion absorbed during the melting process. It has the value of zero everywhere except over the intervals $(T_m - \Delta T/2)$ and $(T_m + \Delta T/2)$. More importantly, its integral over the range of all temperatures is equal to 1; therefore, by multiplying $D(T)$ by L, the energy balance through the phase transition is ensured.

Using the two functions described by Eqs. (3) and (4), the modified heat capacity, $C_p(T)$, of the PCM is defined as follows:

$$C_p(T) = C_{p,s} + B(T)\left(C_{p,l} - C_{p,s}\right) + L \cdot D(T) \tag{5}$$

where s and l refer to the solid and liquid phases of the PCM, respectively. More detail about this application of the modified heat capacity method can be found in [25]. It is important to note that methods (both enthalpy and modified heat capacity) using a mushy zone for the modeling of phase change heat transfer on a fixed grid are not new [26]; they have been well validated analytically and experimentally over the years, with applications ranging from the historical Stefan problem [27] to PCM composites [28] and melting with natural convection [29, 30] to just name a few.

The equations presented above were implemented using COMSOL modules. Heat transfer in fluids as well as laminar flow were applied to the air domains, while heat transfer in solids was applied to the PCM domains. In the air domains, inlet velocity and constant temperature boundary conditions were used at the inlet of the heat exchanger, and open outlet and zero conductive heat flux boundary conditions were used at the outlet. Symmetry and no-slip wall conditions were applied as appropriate to the rest of the boundaries in the computational domain.

2.3 Numerical resolution

The previously presented 3D geometry was created in COMSOL Multiphysics 5.0. The PCM and air properties given in Tables 1 and 2, along with the aforementioned initial and boundary conditions, were incorporated in the numerical model. The expressions of the liquid fraction, $B(T)$, and the Gaussian function, $D(T)$, were programmed within COMSOL through user-defined functions for a temperature interval, ΔT, of 3 K. A Previous study [29] has shown that smaller values of ΔT result in a better agreement between the numerical and experimental PCM melting rates; however, this comes at the expense of a larger number of mesh elements and longer computation times. Therefore, in the present study, ΔT was set equal to 3 K to allow faster simulations on a less dense mesh, thus facilitating the execution of numerous simulations for this parametric study. The heat transfer in solids (PCM), in fluids (air) and the laminar flow (air) physics were implemented and coupled within COMSOL. This enabled the numerical modelling of conduction and convection within the system for the different geometrical properties and operating conditions listed in Table 3.

In order to provide an accurate independent mesh solution and limit the overall calculation time, a swept quadrilateral mesh was used for the studied geometry with an additional boundary layer mesh (4 layers) applied to the air domains as it can be seen in Fig. 2.

Based on a mesh independence study presented in [31], it was found that a total number of 21,480 (16 × 16 × 40) quadrilateral elements provided a sufficient level of accuracy in terms of PCM melting temperature and heat transfer rate. Therefore, the same mesh was used in the current study. In total, 12 simulations were completed for 10 simulated hours each. The computation time varied between 4 h and 27 h for the configurations when running on a workstation with 32 cores clocked at 2.4 GHz and 128 GB of RAM.

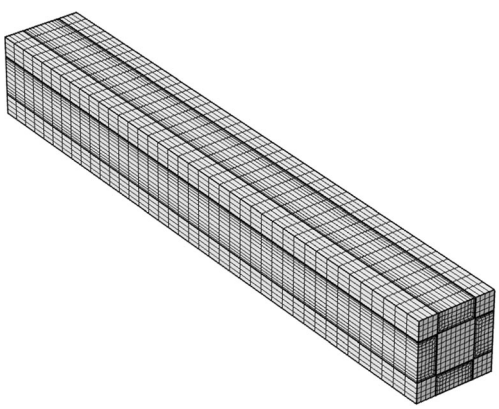

Fig. 2 The three-dimensional section of the modelled PCM-air heat exchanger geometry with (16 × 16 × 40) quadrilateral elements

3 Results and discussion

As previously mentioned, this study explores the dependence of the heat transfer rate on inlet air velocity and temperature as well as the channel size in a cubic PCM-air heat exchanger. The heat transfer rate, Q, is defined by Eq. (6), where $A_{air.ch}$ is the cross sectional area of one air channel and $N_{air.ch}$ is the number of air channels in the full 30 × 30 × 30 cm^3 heat exchanger (see Table 3); ρ, C_p and u_{in} are the density, heat capacity and velocity of the incoming air respectively, and $(T_{in,air} - T_{out,air})$ is the difference between the inlet and outlet air temperatures. The heat transfer rate is driven by the outlet temperature which is calculated through the transient simulation in COMSOL, as the other parameters vary only slightly over 10 h of simulation time.

$$Q = A_{air.ch} N_{air.ch} \rho C_p u_{in} \left(T_{in,air} - T_{out,air}\right) \tag{6}$$

From Eq. (6), the heat flux at the PCM-air interface is defined as:

$$q'' = Q / A_{PCM-air} \tag{7}$$

where $A_{PCM-air}$ is the total surface area of the PCM-air interface for the entire 30 × 30 × 30 cm^3 heat exchanger (see Table 3).

In order to better understand the central "rate problem" in this study, the effect of several variables were explored as the heat transfer rate depends on a variety of factors. Figures 3, 4, and 5 depict the spatial distribution of temperature and heat flux in the heat exchanger for one individual simulation (4-cm channel size, 70 °C air temperature, and 1 m/s inlet velocity). These figures help to elucidate the physical behavior of the heat exchanger. Figures 6, 7, 8, 9, and 10 display the simulated outlet air temperature (z = 30 cm), heat transfer rate, heat flux, average PCM temperature (taking over the entire PCM volume), melt fraction, and total melting time for all the parameter combinations between channel size, inlet air velocity and temperature (Table 3). On all these figures, a) shows these results for varying channel sizes and inlet velocities for an incoming air temperature of 60 °C, while figures b) show the same configurations but for an incoming air temperature of 70 °C.

3.1 Spatial distribution of temperature and heat flux

Figure 3 shows the spatial distribution of the temperature inside the PCM and air channels at four selected positions along the axial channels axis (z = 0, 10, 20 and 30 cm) and at four selected times for a channel size of 4 cm and an inlet air temperature and velocity of 70 °C and 1 m/s respectively. After 100 min of simulation, and at the inlet of the studied geometry (z = 0 cm), the heat exchanged between the air

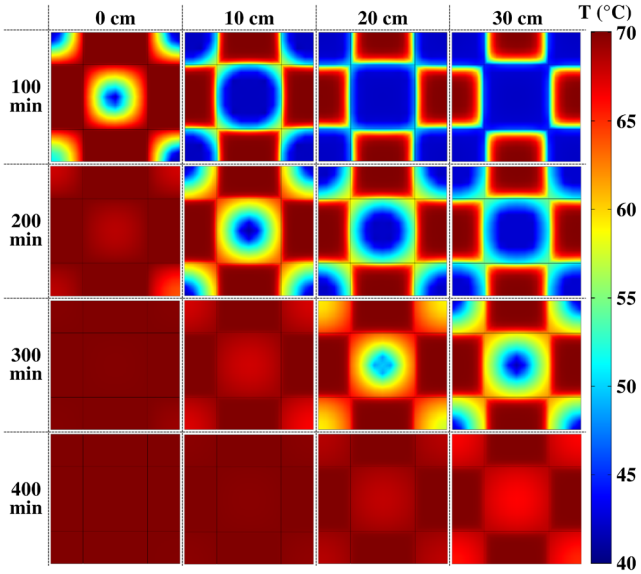

Fig. 3 Spatial distribution of the temperature inside the PCM and air channels at different positions along the channels and different times - 4 cm channel size, 70 °C inlet temperature, and 1 m/s inlet velocity

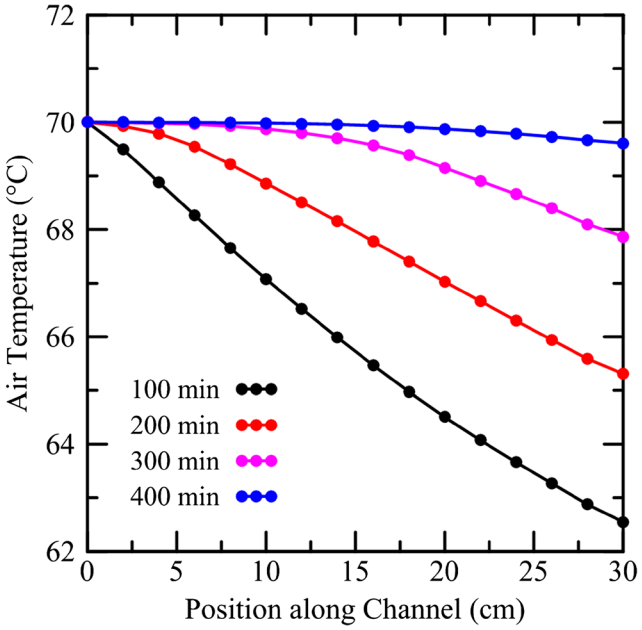

Fig. 5 Spatial evolution of the air temperature along the channel at four selected times - 4 cm channel size, 70 °C inlet temperature, and 1 m/s inlet velocity

entering the system at 70 °C and the PCM results in the increase of the PCM temperature above its melting point almost throughout the whole PCM domain, except in the centre where the PCM is still in solid phase. Moving along the axis (z = 10, 20 and 30 cm), Fig. 3 shows that less PCM is melted, and a lower temperature of the flowing air is achieved mainly at the interface between the two studied domains. As the time proceeds, more heat is stored by the PCM which is illustrated by the increase of its temperature, and a lower temperature gradient exists between the PCM and air channels. It takes about 400 min for the completely melted PCM to reach the temperature of the inlet air, implying that it does not contribute anymore to the cooling of the flowing air.

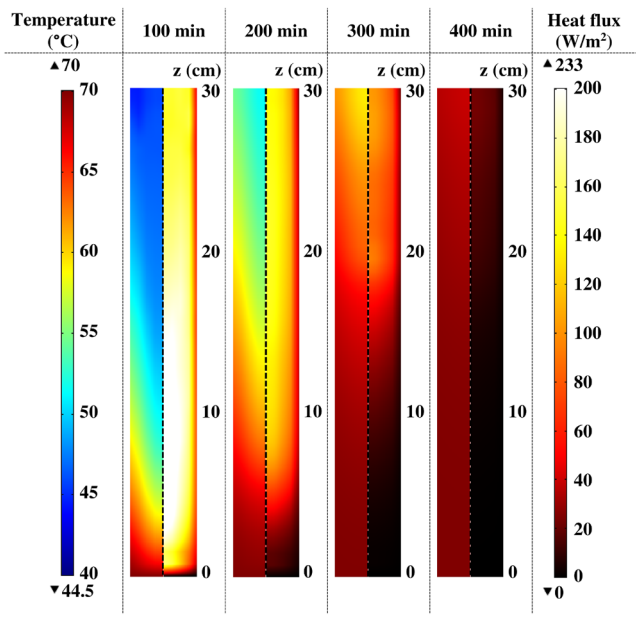

Fig. 4 Temperature and heat flux across PCM-air boundary at different times – 4 cm channel size, 70 °C inlet temperature, and 1 m/s inlet velocity

Figure 4 illustrates the spatial distribution of the temperature (left side) and the linear heat flux (right side) through the planar interface between the PCM and air channels for the full length of the channel. At t = 100 min, it can be seen that the temperature at the interface decreases from 70 °C to about 43.5 °C while moving along the channel axis. This implies that at the inlet of the channel, the completely melted PCM has almost reached the temperature of the incoming air, and there is no heat exchange between the two domains as confirmed by the distribution of the heat flux, which is almost equal to zero. Moving far from the inlet region shows that the interface temperature barely exceeds the melting point of the PCM, which results in a large temperature gradient between the PCM and air domains. Hence, a large amount of heat is exchanged as can be seen from the distribution of the heat flux in the corresponding area. As time proceeds, more heat is stored by the PCM first as latent heat of fusion, and then as sensible heat, resulting in the increase of the interface and overall air temperature along the channel axis. It takes about 400 min to observe a thermal equilibrium between the air and PCM, which is reflected by a zero heat flux throughout the whole planar interface separating the two modelled domains.

3.2 Air temperature evolution

To have a better insight into the evolution of the flowing air temperature, its average value was calculated over the cross-

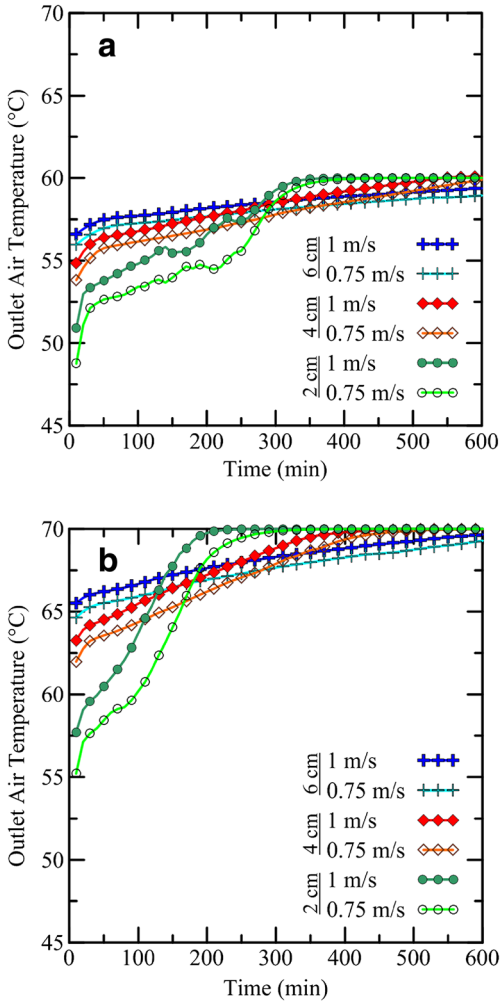

Fig. 6 Outlet air temperature for **a** 60 °C in-flow and **b** 70 °C in-flow

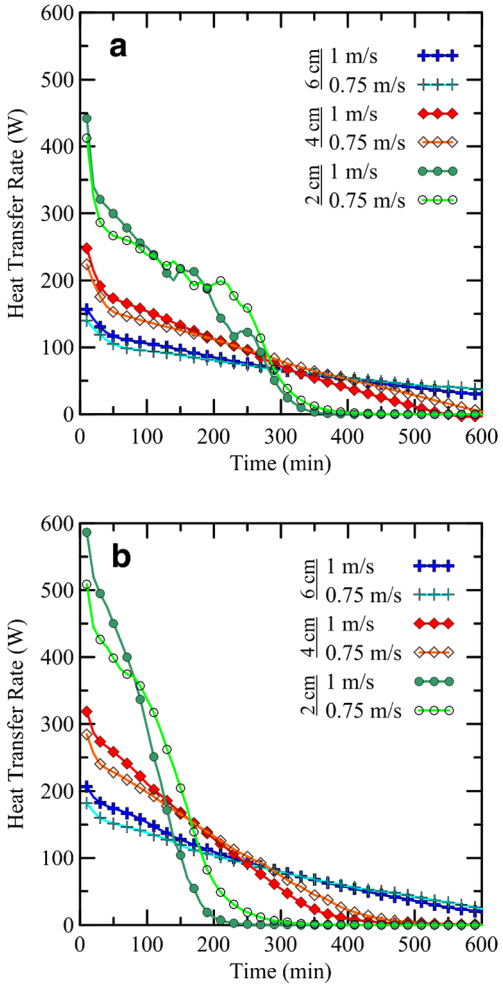

Fig. 7 Heat transfer rate between **a** 60 °C inlet air and PCM, and **b** 70 °C inlet air and PCM

sectional area of the air channel and at incremental positions along the axis of the air channel; the simulation times selected in Figs. 3 and 4 were also used to generate Fig. 5. Recalling that the air channel length is 30 cm, the first 100 min of simulation show that a temperature difference as high as 8 °C is achieved between the inlet and the outlet of the air channel. As time progresses, less heat is stored by the PCM as discussed above, resulting in a smaller difference between the inlet and outlet air temperatures, which reduces to only approximately 0.5 °C after 400 min of simulation time.

From the temporal evolution of the outlet air temperature illustrated in Fig. 6, it can be seen that, initially, a larger difference between the inlet and outlet air temperatures is obtained with a higher incoming air temperature (compare Fig. 6a and b). A second observation that can be made with these plots is that at $t = 0$ min, a better cooling of the outlet air is achieved with a smaller air channel size in both 60 °C and 70 °C simulations. However, as time proceeds, the outlet air temperature rises more quickly towards the incoming air temperature. Indeed, in the case of the 70 °C simulations (Fig. 6b), it takes only 200 and 300 min to observe no difference between $T_{in,air}$ and $T_{out,air}$ for an air channel size of 2 cm, and an inlet air velocity of 1 m/s and 0.75 m/s. A longer interval of time is required for the 4 cm and 6 cm air channel sizes to achieve the same outlet air temperature. A similar trend is also observed in the case of the 60 °C simulations (Fig. 6a) with a smaller effect of the inlet air velocity on the evolution of the outlet air temperature.

3.3 Heat transfer rate and heat flux between the PCM and air

Based on the calculated values of the outlet air temperature depicted above and using Eq. (6), the temporal evolution of the heat transfer rate, Q is presented in Fig. 7. Several observations can be made from the obtained plots. First, the initial heat transfer rate is higher with 70 °C incoming air but decays more quickly than in the 60 °C simulations. This is expected

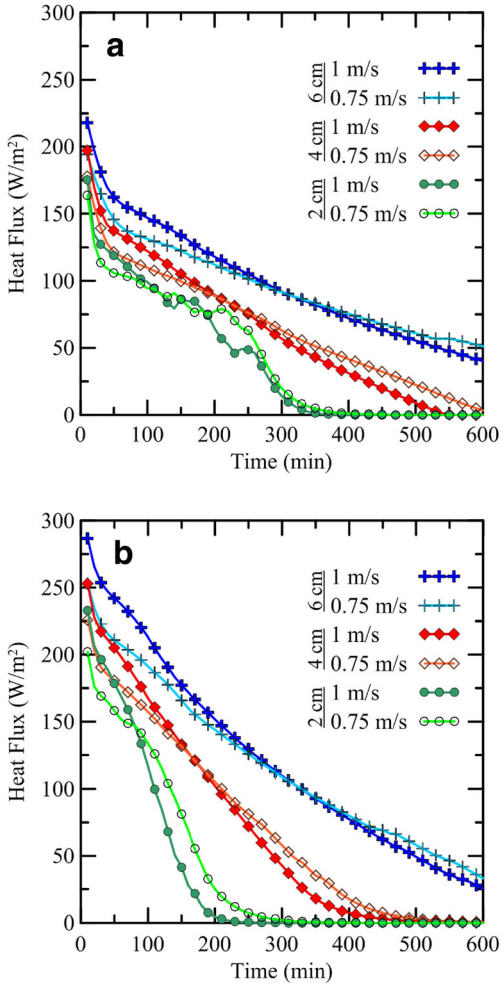

Fig. 8 Heat flux for **a** 60 °C in-flow and **b** 70 °C in-flow

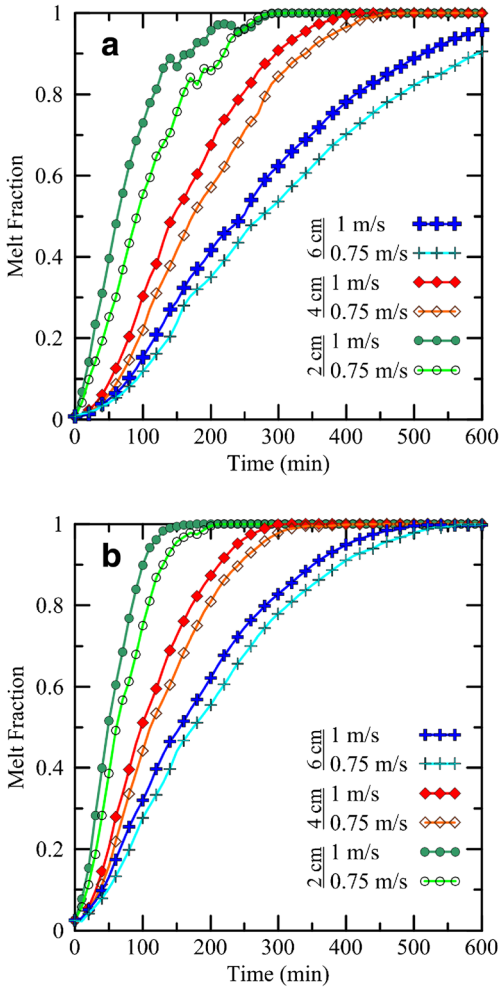

Fig. 9 Melt fraction for **a** 60 °C in-flow and **b** 70 °C in-flow

as the temperature differential between the 70 °C air and initial 20 °C PCM is greater, so the heat transfer rate is expected to be greater as well. The system reached equilibrium more quickly because the PCM melted more quickly, as can be seen from the transient evolution of the melted PCM fraction shown in Fig. 9. Secondly, the size of the channels made the biggest difference in the heat transfer rate. In both 60 °C and 70 °C simulations, the 2-cm channel size started at twice the heat transfer rate of the 4-cm channel size but decayed a lot more quickly. Again, this follows the accelerated melting of the PCM in the 2-cm channel simulations (Fig. 9). Overall, the 2-cm channel size system offer the largest heat transfer area which explains the larger heat transfer rate.

For all channel sizes and inlet temperatures, the 1 m/s inlet velocity started out as the configuration with the highest heat transfer rate, but the 0.75 m/s inlet velocity overtook it later in the simulation. The cross-over occurred increasingly later in the simulation as the channel sizes became larger. The slight fluctuations in the 2-cm channel size in the 60 °C simulations were most likely due to numerical instabilities, which may be a result of not achieving full mesh convergence for the smaller channel sizes; more elements might have been required. However, for consistency, the mesh for the 2-cm needed to have the same number of elements as the other channel sizes.

The heat flux between the air and PCM interfaces illustrated in Fig. 8 did not follow exactly the same pattern as the heat transfer rate. All channel sizes started at roughly the same value in both the 60 °C and 70 °C simulations. Interestingly, the smaller channel offered a slightly lower heat flux (the opposite trend compared to the heat transfer rate results); this can be explained by the fact that with the larger channel, the temperature profile of the air in the channel leads to a greater temperature difference between the wall and the centerline, hence a higher temperature gradient at the wall. Also, as in the heat transfer rate graphs, the smaller the channel size, the more quickly the heat flux decayed to zero. Not suprisingly, the 70 °C simulations (Fig. 8b) started at a higher heat flux than the 60 °C simulations (Fig. 8a), which is a direct result of the greater temperature

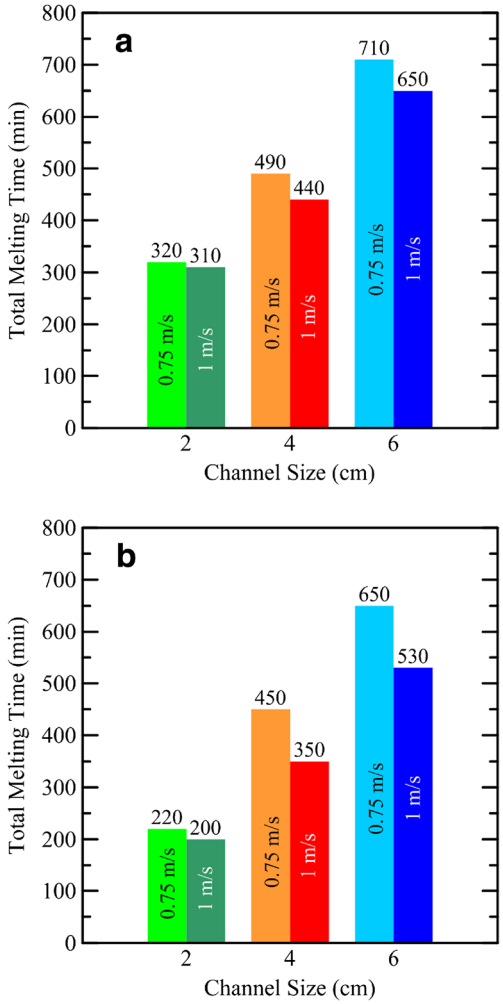

Fig. 10 Total melting time for **a** 60 °C in-flow and **b** 70 °C in-flow

differential. And again, as in the heat transfer rate graphs, the effect of velocity was the same.

3.4 PCM melting fraction and time

The histograms presented in Fig. 10 summarize the total melting times obtained from all conducted simulations. Fig. 10a) (60 °C inlet air temperature) shows that the PCM melted completely after approximately 300 min of simulation time for both 2-cm channel size configurations and after about 500 min of simulation time for the 4-cm channel size configurations. The PCM did not fully melt with the 6 cm channel size configurations after 600 min of simulation time, so extrapolation of the melting fraction curve was used to estimate the total melting time. In Fig. 10b) (70 °C air inlet temperature), the PCM fully melted approximately 100 min faster than the 60 °C simulations for both the 0.75 m/s and 1 m/s inlet velocities for the 2-cm channel size. However, for the 4- and 6-cm channel sizes, the inlet velocity had more impact in the total melting time; this difference is noticeable between the 0.75 and 1 m/s inlet velocities in the-4 cm channel configurations and most pronounced in the 6 cm channel configurations. Hence, the inlet velocity had more of an impact in the 70 °C simulations than in the 60 °C simulations. This comes from the combination of the higher temperature differential driving the heat transfer and melting and the increased convection coefficient within the air channel (for internal convection, the convection coefficient increases with velocity).

4 Conclusion

This paper studied the effect that the geometry and operating conditions of a PCM-air heat exchanger has on the heat transfer rate between incoming hot air and the PCM (dodecanoic acid). Through 10 h of simulated time conducted in COMSOL Multiphysics 5.0, it was determined that the configuration with a channel size of $2 \times 2 \times 30$ cm^3, inlet velocity of 1 m/s, and inlet temperature of 70 °C resulted in the highest heat transfer rate at the beginning of the 10-h simulation and the sharpest rate of decline. Conversely, the configuration with a channel size of $6 \times 6 \times 30$ cm^3, inlet velocity of 0.75 m/s, and inlet temperature of 60 °C resulted in the lowest heat transfer rate between the incoming air and the PCM in the beginning of the simulation but also the slowest rate of decline over the length of the simulation.

Within the configurations studied in these simulations, the size of the channels had the biggest effect on the heat transfer rate between the air and PCM, followed by the incoming air temperature. The inlet velocity had the smallest effect. However, the inlet velocity proved to have a more pronounced effect for the total melting time of the PCM, especially with the higher incoming air temperature of 70 °C. Moreover, the actual heat flux from the air to the PCM was greater for the larger channel size, due to the larger temperature gradients observed at the wall.

From the results of these simulations, the geometry of PCM-air heat exchangers can now be selected by thermal designers to match the HVAC or air energy storage applications from the perspective of heat flux or global heat transfer rate, thus addressing the “rate problem” that is currently limiting most PCM-thermal storage system designs.

Acknowledgements The authors would like to thank Public Work and Government Services Canada (PWGSC), the Natural Science and Engineering Research Council (NSERC) of Canada and the Canada Foundation for Innovation (CFI) for their financial support.

Compliance with ethical standards The author(s) declare that they have no competing interests.

References

1. Pérez-Lombard L, Ortiz J, Coronel JF, Maestre IR (2011) A review of HVAC systems requirements in building energy regulations. Energ Buildings 43:255–268. doi:10.1016/j.enbuild.2010.10.025
2. de Gracia A, Cabeza LF (2015) Phase change materials and thermal energy storage for buildings. Energ Buildings 103: 414–419. doi:10.1016/j.enbuild.2015.06.007
3. Iten M, Liu S, Shukla A (2016) A review on the air-PCM-TES application for free cooling and heating in the buildings. Renew Sust Energ Rev 61:175–186. doi:10.1016/j.rser.2016.03.007
4. Groulx D, C. Kheirabadi a, Desgrosseilliers L, Kabbara M, Azad M, Donaldson A, Joseph A, White MA (2016) working towards solving the rate problem: geometric vs Nano-enhanced PCM solutions. INNOSTORAGE conference, ben-Gurion University of the Negev, beer-Sheva, Israel
5. Vakilaltojjar SM, Saman W (2001) Analysis and modelling of a phase change storage system for air conditioning applications. Appl Therm Eng 21:249–263. doi:10.1016/S1359-4311(00)00037-5
6. Lazaro A, Dolado P, Marin JM, Zalba B (2009) PCM-air heat exchangers for free-cooling applications in buildings: empirical model and application to design. Energy Convers Manag 50:444–449. doi:10.1016/j.enconman.2008.11.009
7. Zalba B, Marín JM, Cabeza LF, Mehling H (2004) Free-cooling of buildings with phase change materials. Int J Refrig 27:839–849. doi:10.1016/j.ijrefrig.2004.03.015
8. Dolado P, Lazaro A, Marin JM, Zalba B (2011) Characterization of melting and solidification in a real scale PCM-air heat exchanger: numerical model and experimental validation. Energy Convers Manag 52:1890–1907. doi:10.1016/j.enconman.2010.11.017
9. Mosaffa AH, Infante Ferreira CA, Talati F, Rosen MA (2013) Thermal performance of a multiple PCM thermal storage unit for free cooling. Energy Convers Manag 67:1–7. doi:10.1016/j.enconman.2012.10.018
10. Labat M, Virgone J, David D, Kuznik F (2014) Experimental assessment of a PCM to air heat exchanger storage system for building ventilation application. Appl Therm Eng 66:375–382. doi:10.1016/j.applthermaleng.2014.02.025
11. Stathopoulos N, El Mankibi M, Santamouris M (2017) Numerical calibration and experimental validation of a PCM-air heat exchanger model. Appl Therm Eng 114: 1064–1072. doi:10.1016/j.applthermaleng.2016.12.045
12. Mankibi ME, Stathopoulos N, Rezaï N, Zoubir A (2015) Optimization of an air-PCM heat exchanger and elaboration of peak power reduction strategies. Energ Buildings 106:74–86. doi:10.1016/j.enbuild.2015.05.023
13. Hed G, Bellander R (2006) Mathematical modelling of PCM air heat exchanger. Energ Buildings 38:82–89. doi:10.1016/j.enbuild.2005.04.002
14. Arzamendia Lopez JP, Kuznik F, Baillis D, Virgone J (2013) Numerical modeling and experimental validation of a PCM to air heat exchanger. Energ Buildings 64:415–422. doi:10.1016/j.enbuild.2013.04.017
15. Kuznik F, Arzamendia Lopez JP, Baillis D, Johannes K (2015) Design of a PCM to air heat exchanger using dimensionless analysis: application to electricity peak shaving in buildings. Energ Buildings 106:65–73. doi:10.1016/j.enbuild.2015.03.046
16. Wert S, Cruickshank CA, Groulx D (2017) Characterization of an Air-PCM Energy Storage Design for Air Handling Unit Applications. ASME 2017 Summer Heat transfer conference - HT2017, Washington
17. Omojaro P, Breitkopf C (2014) Investigating and modeling of simultaneous charging and discharging of a PCM heat exchanger. Energy Procedia 48:413–422. doi:10.1016/j.egypro.2014.02.048
18. Promoppatum P, Yao S-C, Hultz T, Agee D (2017) Experimental and numerical investigation of the cross-flow PCM heat exchanger for the energy saving of building HVAC. Energ Buildings 138:468–478. doi:10.1016/j.enbuild.2016.12.043
19. Antony Aroul Raj V, Velraj R (2011) Heat transfer and pressure drop studies on a PCM-heat exchanger module for free cooling applications. Int J Therm Sci 50:1573–1582. doi:10.1016/j.ijthermalsci.2011.01.025
20. Tay NHS, Belusko M, Bruno F (2012) Designing a PCM storage system using the effectiveness-number of transfer units method in low energy cooling of buildings. Energ Buildings 50:234–242. doi:10.1016/j.enbuild.2012.03.041
21. Arkar C, Vidrih B, Medved S (2007) Efficiency of free cooling using latent heat storage integrated into the ventilation system of a low energy building. Int J Refrig 30:134–143. doi:10.1016/j.ijrefrig.2006.03.009
22. Gowreesunker BL, Tassou SA, Kolokotroni M (2013) Coupled TRNSYS-CFD simulations evaluating the performance of PCM plate heat exchangers in an airport terminal building displacement conditioning system. Build Environ 65:132–145. doi:10.1016/j.buildenv.2013.04.003
23. O'Connor D, Calautit JKS, Hughes BR (2016) A review of heat recovery technology for passive ventilation applications. Renew Sust Energ Rev 54:1481–1493. doi:10.1016/j.rser.2015.10.039
24. Desgrosseilliers L, Whitman CA, Groulx D, White MA (2013) Dodecanoic acid as a promising phase-change material for thermal energy storage. Appl Therm Eng 53:37–41. doi:10.1016/j.applthermaleng.2012.12.031
25. Groulx D, Biwole PH (2014) Solar PV passive temperature control using phase change materials. 15th international heat transfer conference (IHTC-15), Kyoto
26. Voller VR, Prakash C (1987) A fixed grid numerical modelling methodology for convection-diffusion mushy region phase-change problems. Int J Heat Mass Transf 30:1709–1719
27. Ogoh W, Groulx D (2010) Stefan's problem: validation of a one-dimensional solid-liquid phase change heat transfer process. COMSOL conference 2010, Boston
28. Mallow AM, Abdelaziz O, Graham SJ (2016) Thermal charging study of compressed expanded natural graphite/phase change material composites. First Pacific Rim Thermal Engineering Conference, PRTEC, Hawaii's Big Island
29. Kheirabadi AC, Groulx D (2015) The effect of the mushy-zone constant on simulated phase change heat transfer. CHT-15 ICHMT International Symposium on Advances in Computational Heat Transfer, Rutgers University, Piscataway
30. Biwole PH, Eclache P, Kuznik F (2013) Phase-change materials to improve solar panel's performance. Energ Buildings 62:59–67. doi:10.1016/j.enbuild.2013.02.059
31. Herbinger F, Bhouri M, Groulx D (2016) Numerical study of a PCM-air heat exchanger's thermal performance. J Phys Conf Ser 745:032127

Terms and Conditions

Springer Nature journal content, brought to you courtesy of Springer Nature Customer Service Center GmbH (“Springer Nature”).
Springer Nature supports a reasonable amount of sharing of research papers by authors, subscribers and authorised users (“Users”), for small-scale personal, non-commercial use provided that all copyright, trade and service marks and other proprietary notices are maintained. By accessing, sharing, receiving or otherwise using the Springer Nature journal content you agree to these terms of use (“Terms”). For these purposes, Springer Nature considers academic use (by researchers and students) to be non-commercial.
These Terms are supplementary and will apply in addition to any applicable website terms and conditions, a relevant site licence or a personal subscription. These Terms will prevail over any conflict or ambiguity with regards to the relevant terms, a site licence or a personal subscription (to the extent of the conflict or ambiguity only). For Creative Commons-licensed articles, the terms of the Creative Commons license used will apply.
We collect and use personal data to provide access to the Springer Nature journal content. We may also use these personal data internally within ResearchGate and Springer Nature and as agreed share it, in an anonymised way, for purposes of tracking, analysis and reporting. We will not otherwise disclose your personal data outside the ResearchGate or the Springer Nature group of companies unless we have your permission as detailed in the Privacy Policy.
While Users may use the Springer Nature journal content for small scale, personal non-commercial use, it is important to note that Users may not:

1. use such content for the purpose of providing other users with access on a regular or large scale basis or as a means to circumvent access control;
2. use such content where to do so would be considered a criminal or statutory offence in any jurisdiction, or gives rise to civil liability, or is otherwise unlawful;
3. falsely or misleadingly imply or suggest endorsement, approval , sponsorship, or association unless explicitly agreed to by Springer Nature in writing;
4. use bots or other automated methods to access the content or redirect messages
5. override any security feature or exclusionary protocol; or
6. share the content in order to create substitute for Springer Nature products or services or a systematic database of Springer Nature journal content.

In line with the restriction against commercial use, Springer Nature does not permit the creation of a product or service that creates revenue, royalties, rent or income from our content or its inclusion as part of a paid for service or for other commercial gain. Springer Nature journal content cannot be used for inter-library loans and librarians may not upload Springer Nature journal content on a large scale into their, or any other, institutional repository.
These terms of use are reviewed regularly and may be amended at any time. Springer Nature is not obligated to publish any information or content on this website and may remove it or features or functionality at our sole discretion, at any time with or without notice. Springer Nature may revoke this licence to you at any time and remove access to any copies of the Springer Nature journal content which have been saved.
To the fullest extent permitted by law, Springer Nature makes no warranties, representations or guarantees to Users, either express or implied with respect to the Springer nature journal content and all parties disclaim and waive any implied warranties or warranties imposed by law, including merchantability or fitness for any particular purpose.
Please note that these rights do not automatically extend to content, data or other material published by Springer Nature that may be licensed from third parties.
If you would like to use or distribute our Springer Nature journal content to a wider audience or on a regular basis or in any other manner not expressly permitted by these Terms, please contact Springer Nature at

onlineservice@springernature.com